01 Aug 1994

Effect of Carrier Gas Pressure on Condensation in a Supersonic Nozzle

Barbara Ellen Wyslouzil

Gerald Wilemski
Missouri University of Science and Technology, wilemski@mst.edu

M. G. Beals

Michael B. Frish

Recommended Citation

B. E. Wyslouzil et al., "Effect of Carrier Gas Pressure on Condensation in a Supersonic Nozzle," *Physics of Fluids*, vol. 6, no. 8, pp. 2845-2854, American Institute of Physics (AIP), Aug 1994.
The definitive version is available at https://doi.org/10.1063/1.868107

Effect of carrier gas pressure on condensation in a supersonic nozzle

B. E. Wyslouzil,[a] G. Wilemski,[b] M. G. Beals, and M. B. Frish[c]
Physical Sciences Inc., 20 New England Business Center, Andover, Massachusetts 01810

(Received 30 November 1993; accepted 14 March 1994)

Supersonic nozzle experiments were performed with a fixed water or ethanol vapor pressure and varying amounts of nitrogen to test the hypothesis that carrier gas pressure affects the onset of condensation. Such an effect might occur if nonisothermal nucleation were important under conditions of excess carrier gas in the atmospheric pressure range, as has been suggested by Ford and Clement [J. Phys. A **22**, 4007 (1989)]. Although a small increase was observed in the condensation onset temperature as the stagnation pressure was reduced from 3 to 0.5 atm, these changes cannot be attributed to any nonisothermal effects. The pulsed nozzle experiments also exhibited two interesting anomalies: (1) the density profiles for the water and ethanol mixtures were shifted in opposite directions from the dry N_2 profile; (2) a long transient period was required before the nozzle showed good pulse-to-pulse repeatability for condensible vapor mixtures. To theoretically simulate the observed onset behavior, calculations of nucleation and droplet growth in the nozzle were performed that took into account two principal effects of varying the carrier gas pressure: (1) the change in nozzle shape due to boundary layer effects and (2) the variation in the heat capacity of the flowing gas. Energy transfer limitations were neglected in calculating the nucleation rates. The trend of the calculated results matched that of the experimental results very well. Thus, heat capacity and boundary layer effects are sufficient to explain the experimental onset behavior without invoking energy transfer limited nucleation. The conclusions about the rate of nucleation are consistent with those obtained recently using an expansion cloud chamber, but are at odds with results from thermal diffusion cloud chamber measurements.

I. INTRODUCTION

Supersonic nozzles and shock tubes have been used for over 50 years to investigate the condensation of rapidly cooled vapor mixtures, and a large body of information has been amassed.[1–14] One of the most important concerns is to understand how and why the observed onset of condensation varies with different experimental conditions. The onset of condensation is the point in the expanding flow where the density, pressure, and temperature begin to deviate from the isentropic values. Aside from the enormously difficult theoretical task of predicting the onset of condensation from well-founded physical principles, there remain perplexing differences in onset conditions measured by different investigators that are too large to be accounted for by experimental errors. While some of these differences can surely be explained in terms of the nonequilibrium conditions developed in extremely rapid molecular beam and free jet expansions compared to the much gentler expansions found in Laval nozzles and shock tubes, many experimental results found with these latter devices also show unexplained differences in the onset temperature of condensation. Examples can be readily cited for the condensation of water,[9,10] argon,[11–13] and nitrogen.[14] Steinwandel[14] has suggested that these variations may be understood in terms of the influence of the cooling rate and carrier gas pressure on the nucleation kinetics. Cooling rates for shock tubes (10 to 50 K/ms) are much smaller than those of Laval nozzles (1 to 10 K/μs) and free jets (>10 K/μs), and the extent of undercooling measured in these devices generally increases with increasing cooling rate. The effect of carrier gas pressure is harder to discern because the experiments cited were performed over ranges of stagnation pressures that generally differed from investigator to investigator. Moreover, no experiments with fixed condensible pressure and varying stagnation pressure were reported. This makes it difficult to isolate the effect of carrier gas pressure on nucleation and condensation rates, since the latter quantities are also strongly affected by changes in the condensible pressure.

Our recent experiments explore the effect of carrier gas pressure on the onset of condensation in the atmospheric pressure range. As noted, this factor has not been systematically varied before, but it can qualitatively account for a shift in onset temperature.[14] In principle, larger nucleation and growth rates (and higher onset temperatures) are achievable at higher carrier gas pressures because "hot" clusters can be more rapidly thermalized than at low pressures.[15–22] The latent heat of condensation significantly raises the internal energy of a cluster formed by monomer addition. Until this excess energy is removed via gas-cluster collisions, the cluster is prone to decay by reemitting a monomer. Barschdorff[10] previously observed a change in onset temperature due to this effect for high mass fractions of condensible vapor. Recently, Ford and Clement[19,20] suggested that a similar effect on nucleation rates might be observable under conditions of excess carrier gas at about 1 atm. Their suggestion was one of the principal motivations of this work, although their earlier conclusions[19,20] have recently been tempered.[21]

[a]Present address: Chemical Engineering Department, Worcester Polytechnic Institute, Worcester, Massachusetts 01609.
[b]Present address: Lawrence Livermore National Laboratory, Livermore, California 94550.
[c]Present address: PSI Environmental Instruments, 20 New England Business Center, Andover, Massachusetts 01810.

 1070-6631/94/6(8)/2845/10/$6.00

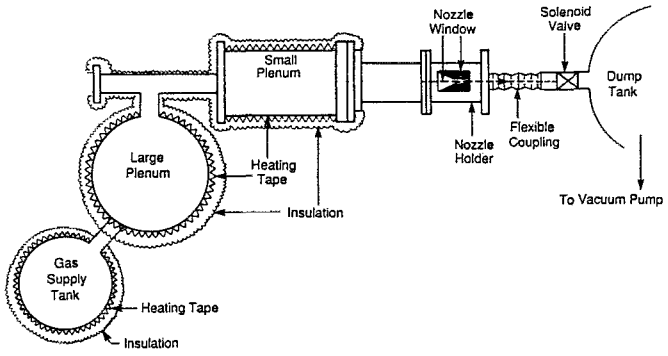

FIG. 1. Flow system schematic.

The recent experimental evidence for a carrier gas pressure effect in other types of experiments is contradictory. In diffusion cloud chamber experiments, Katz *et al.*[23] found a decrease in nucleation rate of four to five orders of magnitude with increases of carrier gas pressure from 100 to 2000 Torr. An opposite, but smaller, trend was observed in flow diffusion chamber experiments by Anisimov and Vershinin.[24] Recently, Wagner, Strey, and Viisanen,[25] using an expansion cloud chamber, reported no intrinsic effect of carrier gas pressure on the nucleation process. Our own preliminary findings[26] were consistent with those of Wagner, Strey, and Viisanen.[25]

The goal of our work was to determine if a reduction in carrier gas pressure would delay condensation onset to a lower temperature in the nozzle because of strong nonisothermal nucleation effects. The higher nucleation rates achieved in a nozzle should enhance such an effect because the time for thermal equilibration with the background gas between monomer incorporation is reduced. In our experiments, we have not observed a significant variation in the onset of condensation (with a fixed low initial concentration of water or ethanol vapor) accompanying a decrease in the carrier gas pressure from roughly 1 to 0.2 atm at the onset of condensation. Thus, our results provide evidence that nonisothermal nucleation effects are unimportant for excess carrier gas pressures in the atmospheric range even at the high nucleation rates found in nozzles.

II. EXPERIMENTAL APPARATUS AND DATA ANALYSIS

Our experimental apparatus is illustrated in Fig. 1. It consists of an intermittent, low Mach number, supersonic Laval nozzle that is equipped to do Mach–Zender interferometry. The two-dimensional nozzle, with a 0.5×1.23 cm^2 ($h\times w$) throat, is defined by two carefully machined aluminum blocks enclosed between two parallel aluminum walls. Each aluminum wall contains a 5 cm diameter interferometer quality window. The nozzle has an 11:1 contraction upstream of the throat and the 7.9 cm long supersonic portion consists of straight, diverging walls with an exit-to-throat area ratio of about 1.37 that yields a maximum Mach number of 1.72 for a perfect diatomic gas. The pressure within the nozzle is measured at a 450 μm diameter orifice located in the upper nozzle block about 0.6 cm downstream of the nozzle's geometric throat. When the gas in the nozzle is at rest this pressure reading is the stagnation pressure. The position of the pressure tap is arbitrarily assigned the value $x=0.0$.

Two heated plenum chambers feed the nozzle which exhausts into a vacuum dump tank. These are in turn fed by a gas supply tank which holds enough gas to refill the large plenum for 50 or more 300 ms runs. Experiments are started by opening a solenoid valve located well downstream of the nozzle. During supersonic flow this geometry assures that the valve has no influence on the flow through the nozzle. The gas mixtures are prepared by accurately metering the desired amount of condensible vapor from a pressurized saturator into the previously evacuated supply tank or plenums and then adding the required amount of N_2 carrier gas. Two high accuracy capacitance pressure transducers are used to cover the required pressure ranges. The large plenum (250 liters) is heated to within 5 K of the desired stagnation temperature and contains enough gas to maintain the initial temperature to within 0.2% during the run. This plenum feeds the small plenum (10 liters) which, at the start of the run, contains all of the gas which will flow through the nozzle during that run. The temperature of this gas is maintained within 1 K of the desired stagnation temperature.

During the steady supersonic flow periods of several hundred milliseconds, one-dimensional density, temperature, and pressure gradients are established in the nozzle. Typical cooling rates are about 0.6 K/μs. Temperatures between 220 and 260 K are achieved in the condensation zone downstream of the nozzle throat. The interferometry data yield a relative density profile in the nozzle while pressure measurements made before and during flow at the pressure tap fix the absolute value of the density ratio. Assuming that no condensation has occurred upstream of the orifice, the pressure p is related to the local density ρ by the isentropic gasdynamic relationship $\rho/\rho_0=(p/p_0)^{1/\gamma}$, where the subscript "0" refers to the stagnation conditions in the plenum tank, and γ is the usual ratio of specific heats. Because these flow times are so short, it is not possible to simultaneously measure pressure along the nozzle centerline using a Pitot tube as described by other experimentalists.[3–5]

The basic theory of Mach–Zehnder interferometry is well described in the literature.[27–29] Its primary feature is that the fringes comprising the interference pattern when the gas is flowing are shifted in position when compared with those created when the gas is stagnant. Each fringe is usually assigned a number counted from an arbitrary origin within the nozzle, denoted by x_0. The fringe shift, or local change in the fringe number at position x when comparing flow and no-flow situations, is given by

$$k(x)=(\beta L/\lambda\rho_s)\Delta\rho, \tag{1}$$

where $\rho(x)$ is the local density during the flow, $\Delta\rho=\rho(x)-\rho_0$, β/ρ_s is the Gladstone–Dale constant determined by the gas used,[27,28] L is the path length through which the light passes in the nozzle, λ is the wavelength of the light, and ρ_s is the gas density at 1 atm and 273.15 K. Clearly, each unit fringe shift, i.e., one for which the position

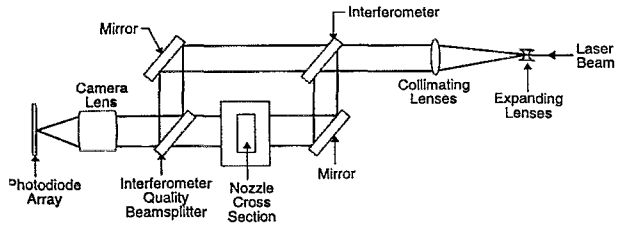

FIG. 2. Schematic of Mach–Zehnder interferometer.

of a fringe recorded during flow moves to the position that the next fringe occupied during no-flow, corresponds to a density change of $\lambda\rho_s/\beta L$. By measuring $k(x)$, Eq. (1) can be inverted to yield the density as a function of position

$$\frac{\rho(x)}{\rho_0}=\left(\frac{RT_0}{\mu p_0}\right)\left(\frac{\rho_s\lambda}{\beta L}\right)[k(x)-k(0)]+\left(\frac{p(0)}{p_0}\right)^{1/\gamma}, \tag{2}$$

where R is the molar gas constant, T_0 is the stagnation temperature, μ is the average molecular weight of the gas mixture, and β/ρ_s is an average Gladstone–Dale constant determined with the mass fraction f_i of each component: $\beta/\rho_s=\Sigma f_i\beta_i/\rho_{is}$.

As illustrated in Fig. 2, the fringe patterns produced in our interferometry setup are detected using a photodiode array rather than by the more traditional method of double exposure photography. The voltage output from the array is collected from 256 of the diodes and recorded in about 14 ms using an Apple computer. The computer samples and stores these data twice for each run: once immediately before the flow begins, and again approximately 250 ms later, when the flow has attained steady state conditions. The computer also samples the pressure at these times, to determine an absolute density ratio for the flow at $x=0$.

The time-varying voltage signals generated by each of the two interference patterns are oscillatory in appearance. The intensity $I(x)$ of each interference pattern varies with position as

$$I(x)=1-\sin\,\pi m(x), \tag{3}$$

where $m(x)$ is a function of the interferometer setup and any density gradients in the system. To calculate the density-ratio profile, the sampled intensity patterns from each of the two trials are, in principle, added together to simulate doubly exposed photographs, and the areas of fringe overlap or cancellation are located. If the no-flow interference pattern is described by the functions $I_1(x)$ and $m_1(x)$, and the pattern with flow by $I_2(x)$ and $m_2(x)$, then the intensity which results from adding the two signals is

$$I(x)=I_1(x)+I_2(x)=2-[\sin\,\pi m_1(x)+\sin\,\pi m_2(x)], \tag{4}$$

which can be rewritten as

$$I(x)=2(1-\sin\{\pi[m_1(x)+m_2(x)]/2\}\times\cos\{\pi[m_1(x)-m_2(x)]/2\}). \tag{5}$$

The resulting intensity variation is similar to the apparent amplitude modulation or "beating" that is observed when two sinusoidal signals of slightly different frequencies are added together. The sine term in Eq. (5) contains a high-frequency oscillation which is modulated by the low-frequency cosine term. In the present case, the cosine term mathematically describes the Moiré pattern that results from photographically combined interferograms. When the cosine term equals unity, i.e., when $m_1(x)-m_2(x)=2K$, the peaks overlap and $k(x)=K$. In contrast, when $m_1(x)-m_2(x)=2K+1$, the fringe patterns are exactly 180° out of phase and $k(x)=(2K+1)/2$. Therefore the fringe shift function $k(x)$ is given simply by

$$k(x)=[m_1(x)-m_2(x)]/2. \tag{6}$$

Since $k(x)$ is determined entirely by the functions $m_1(x)$ and $m_2(x)$, there is no need to actually add $I_1(x)$ and $I_2(x)$. Instead, by finding the positions of the relative maxima and minima in the measured interferometer signals and counting fringes relative to an arbitrary origin, $m_1(x)$ and $m_2(x)$ are calculated directly from the measured values of $I_1(x)$ and $I_2(x)$. Equation (6) is then used to calculate $k(x)$, and $\Delta\rho$ follows directly from Eq. (1). In practice, the values of $m(x)$ are determined by adjusting the interferometer to generate fringes which are spaced widely enough to be just resolvable by the photodiode array with one complete cycle defined by approximately five points. The maxima and minima of the two intensity functions are located relative to the position of the pressure sensing orifice, and appropriate fringe-shift values are assigned to them. These discrete points are sufficiently close together that $m(x)$ can be accurately approximated at any other position by a linear interpolation between them. Because the intensity function is sampled only at a limited number of discrete points, the precise maxima or minima are, in general, not likely to have been detected. A good estimate of their true location is obtained by finding the location of the extremum of a parabola that has been fit through the closest three points.

Deviations from isentropic flow caused by latent heat release, when sufficiently large, can be detected with the interferometer by comparing density-ratio profiles obtained under conditions of dry flow to those obtained with condensation. The temperature profile of the expanding/condensing flow is obtained by integrating the diabatic gasdynamics equations using the measured dry and wet density profiles as input data, following a procedure similar to that of Wegener and Pouring.[3,9] The first step in calculating the heat release is to calibrate the effective shape of the nozzle using the dry density measurements and the isentropic gasdynamic equations in the form

$$M^2(x)=\frac{2}{\gamma-1}\left[\left(\frac{\rho_0}{\rho(x)}\right)^{\gamma-1}-1\right], \tag{7}$$

$$\left(\frac{A(x)}{A^*}\right)^2=\frac{1}{M^2(x)}\left[\frac{2}{\gamma+1}\left(1+\frac{\gamma-1}{2}M^2(x)\right)\right]^{(\gamma+1)/(\gamma-1)}, \tag{8}$$

where γ is the specific heat ratio, $M(x)$ is the local Mach number, and $A(x)$ is the effective nozzle cross-sectional area at x. The superscript "*" denotes conditions at the nozzle throat. Although the approximate shape of the nozzle is

known from its design, boundary layers in a nozzle as small as ours significantly change both the location of the throat and the effective shape of the nozzle downstream. Thus calibrating the effective nozzle shape at each pressure is extremely important. Next, using the area ratio profile calculated from Eq. (8) with the appropriate condensing flow density profile, the temperature, pressure, and condensate mass fraction curves are calculated by numerically integrating the gasdynamics equations for diabatic flow as described in the Appendix.

There are a few practical difficulties in implementing the scheme which must be addressed. Derivatives of the measured density curves are required in deriving the other properties of the flow. The noise in these data is amplified by numerical differentiation, but smoothing the raw density data using a five point cubic interpolation deals with this quite effectively. The bigger sources of uncertainty are small (<2%) changes in the measured density profiles between the true isentropic N_2 expansions and the isentropic portion of the condensing flow. Calculating an equivalent "wet isentrope," i.e., an ideal noncondensing moist flow expanding along the area ratio defined by the dry flow but corrected for any differences in γ, does not correct this discrepancy. Rather, it is the result of differences in the measured pressure ratios at $x=0$ which vary slightly at the same total stagnation pressure as the mixture composition changes. The shifts are opposite for H_2O and for ethanol. The water data generally lie below the dry or "wet isentropic" curves while the ethanol curves are generally above. Except for this slight shift, the overall shape of the relative density profile is very close to the dry N_2 density profile. One possible reason for this slight shift is a small change in the boundary layer due to differences in the viscosity and density of the condensible gas mixture from the dry N_2 case.

We have not seen any discussions of this problem in the literature. We would not expect Wegener *et al.*[4] to have observed such a shift because of their low initial concentrations of condensible vapor. When we approached their conditions the discrepancy also vanished. If, as a first approximation, we apply incompressible boundary layer theory to the nozzle, the boundary layer thickness δ should grow as

$$\delta/l \propto (\mathrm{Re})^{-1/2}, \tag{9}$$

where $\mathrm{Re}=lu\rho/\eta$, l is distance in the nozzle from the start of the boundary layer, and η is the viscosity. At a given position in the nozzle, a thinner boundary layer implies a more rapid expansion and therefore a lower pressure ratio at $x=0$. Both density and viscosity change with the mixture composition. In the most extreme case for water (17.2 Torr H_2O at 0.5 atm total pressure) we estimate the change in the boundary layer thickness relative to pure N_2 is

$$\delta_{\mathrm{dry}}/\delta_{\mathrm{wet}}=(\rho_{\mathrm{wet}}/\rho_{\mathrm{dry}})^{1/2}(\eta_{\mathrm{dry}}/\eta_{\mathrm{wet}})^{1/2}=1.004, \tag{10}$$

where the relative density of the water mixture to N_2 is taken as

$$(\rho_{\mathrm{wet}}/\rho_{\mathrm{dry}})=(M_{\mathrm{wet}}/M_{\mathrm{dry}})=27.5/28. \tag{11}$$

The viscosity of the water mixture at 250 K, $\eta_{\mathrm{wet}}=0.0151$ mPa s, is approximated using Wilke's method[30] with pure component viscosities of 0.0155 mPa s for N_2 (Ref. 31) and 0.008 mPa s for H_2O (Ref. 32). This slight change in the boundary layer thickness cannot explain the observed difference in the pressure ratios which correspond to a difference in area ratio of 1.003 since the boundary layer itself is only about 0.5% of the height of the channel. Rather we suspect the position of the virtual throat changes slightly with changes in the mixture composition, but we are not in a position to calculate this region of the nozzle in detail.

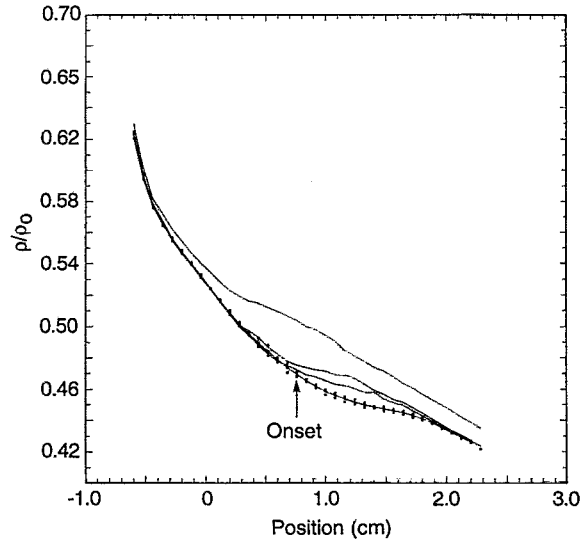

FIG. 3. Illustration of slowly decaying transient during pulsed nozzle operation with condensible vapor present. Density profiles correspond to averages of shots 1–5 (top), 6–10, 11–15, and 20–40 (bottom). The points correspond to the data used to calculate the steady state density profile. The data presented here represent an extreme case.

In light of this discrepancy, let us calculate the worst case error estimate introduced by this uncertainty. For water at 17.22 Torr and 0.5 atm total pressure, $p(0)/p_0=0.442$ for the condensing flow and $p(0)/p_0=0.449$ on the N_2 isentrope. Since $T(0)=T_0[p(0)/p_0]^{(\gamma-1)/\gamma}$, this difference leads to an uncertainty in the temperature of less than 1 K depending on which pressure reading we believe. Currently we deal with this discrepancy by shifting slightly all of the measured condensing flow data to the corresponding "wet isentropic" values, before proceeding with the integration. If we were to assume the correct pressure reading is that measured during the "wet" run rather than the dry we would shift both the onset temperatures and the onset pressures slightly, but the resulting values would still define essentially the same $T-p$ onset line.

A more subtle problem in these experiments involved a rather long term transient associated with the initial shots in a set of condensing flow runs. This transient does not exist in the dry N_2 experiments. Figure 3 illustrates the transient by plotting the average density ratios of shots 1–5, 6–10, 11–15, and the steady state average of shots 20 to 40. Clearly, the averages of the first three sets of shots display significantly higher density ratios and an earlier onset of condensation. Removing these transient data before further analysis greatly enhanced the repeatability of the experiments and our

agreement with other researchers. The transient may be related to the location of the valve, downstream of the nozzle. With this geometry the nozzle walls are in contact with condensible vapor between periods of flow. If a condensate layer forms on the walls, it may take many pulses before this layer affects the flow in a reproducible manner. This transient was usually longer for water than ethanol and for high stagnation pressures than low. While we have no definitive explanation for this transient behavior, we mention it to alert other investigators using a similar pulsed nozzle apparatus.

III. EXPERIMENTAL RESULTS AND DISCUSSION

Most experimental measurements of condensation in supersonic nozzles are experiments at constant stagnation pressure with varying condensible vapor pressure. We conducted such experiments to confirm that our supersonic nozzle results are consistent with those of other workers whose results were generated using different detection techniques in other nozzles. The results for ethanol are shown in Fig. 4(a), where they are compared to the nozzle data of Wegener, Clumpner, and Wu[4] and Dawson *et al.*[33] as well as the shock tube results of Peters.[34] Figure 4(a) also includes the diffusion cloud chamber results of Franck and Hertz[35] and Katz and Ostermeier.[36] Our results are consistent with both other sets of nozzle experiments and the shock tube results. Onset in the diffusion cloud chamber, on the other hand, occurs at lower supersaturations and reflects the much lower nucleation and cooling rates typical of these experiments. Figure 4(b) shows our results for water along with the nozzle results of Pouring,[9,37] Roberts,[38] Stein and Moses,[39] and Stein.[40] Once again the agreement with similar experiments is very good. A detailed discussion of these results, along with models that consider nucleation and droplet growth will be presented in a separate paper.[41] Of primary interest here are the results unique to the current work, i.e., the results of experiments in which the initial pressure of the condensible species, p_c, was constant (17.2 Torr H_2O or 12.8 Torr ethanol) but the pressure of the carrier gas was varied significantly. The interest in this work was sparked by conflicts in both recent theoretical predictions[19–21] and experimental results.[23–26] The most pronounced pressure effects have been observed in the thermal diffusion cloud chamber. In the supersonic nozzle we are able to look at nucleation occurring over a range of pressures corresponding to a change of nucleation rate of about 3 orders of magnitude in the cloud chamber. Furthermore, our modeling indicates that changes in the nucleation rate of a factor of 10 are equivalent to a change in the onset temperature of 3 K. Thus our experiments should easily be sensitive to changes of 10^2 in the nucleation rate.

Typical temperature profiles obtained by integrating the diabatic gasdynamics equations are shown in Fig. 5 for the extreme cases of $p_0=0.5$ and 3 atm and a fixed water vapor pressure of 17.2 Torr. The vertical displacement of the results is due to the increase in the boundary layer thickness at the nozzle walls with a sixfold decrease in pressure. In effect the nozzle shape changes slightly, giving rise to a gentler expansion at low pressure. The derived area ratios as a function of pressure in Fig. 6, illustrate this effect more clearly and demonstrate that the position of the virtual throat, the position

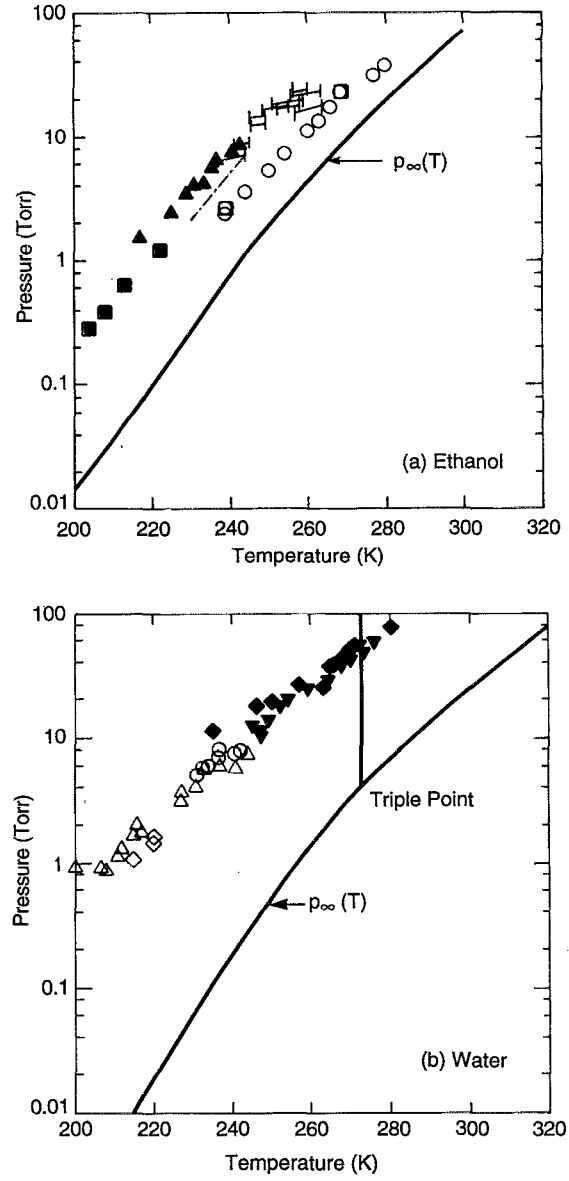

FIG. 4. (a) Onset of ethanol condensation in the supersonic nozzle: current work, ▲; Wegener *et al.* (Ref. 4), ■; Dawson *et al.* (Ref. 33), —; shock tube results of Peters (Ref. 34), ——; diffusion cloud chamber results are Franck and Hertz (Ref. 35), ○; Katz and Ostermeier (Ref. 36), □. (b) Onset of water condensation in the supersonic nozzle. Current work, ○; Pouring (Ref. 37), △; Roberts (Ref. 38), ▼; Stein and Moses (Ref. 39), ◆; Stein (Ref. 40), ◇. The equilibrium vapor pressures for the pure components are indicated by $p_\infty(T)$.

where $A/A^*=1$, can also change slightly. In Fig. 5, we also note the stronger departure of the wet temperature profile from the isentrope as well as the higher peak temperature for the low pressure case. These are consequences of the reduced heat capacity of the lower pressure gas, since condensation adds roughly the same amount of heat to each flowing gas stream. The location of onset is also affected by changes in the heat capacity of the gas stream. This is discussed in Sec. IV. For the experimental results of Fig. 5, onset occurred between $x=1$ and 1.5 cm.

The onset of condensation in a nozzle is difficult to define in a rigorous sense because it depends on the detection

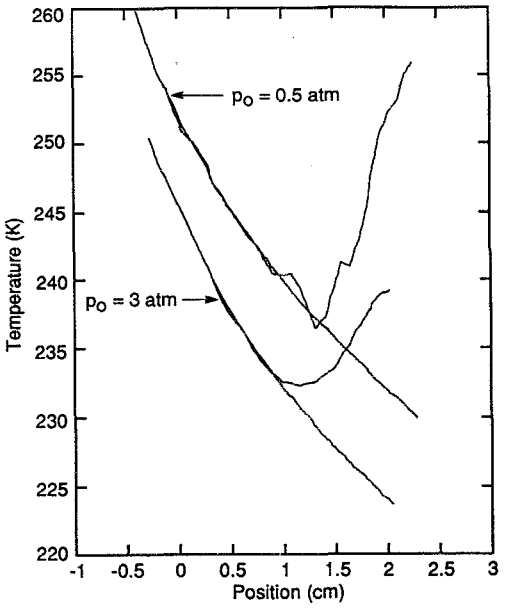

FIG. 5. Integrated temperature profiles for 17.2 Torr H_2O condensing from streams with p_0=0.5 and 3 atm.

technique and the experimental apparatus.[42] The simple statement that onset corresponds to a "significant deviation" from the noncondensing flow needs to be quantified. For example, in their nozzle experiments, Wegener *et al.*[3–5,9] chose the conditions of onset to correspond to a condensed mass ranging from $g=10^{-4}$ to $g=10^{-3}$ depending on the species of interest (water or ethanol). Alternatively, Young[7] used the lowest temperature reached in the expanding flow. In our experiments defining onset is made more difficult when total pressure is low because the interferograms are of poorer quality, and the integrated results become very noisy. At the highest pressures, on the other hand, deviations from the isentrope proceed gradually and again introduce some level of uncertainty. For our analysis and subsequent comparisons to theory we have chosen to define the onset temperature as that temperature at which the condensing flow deviates consistently from the noncondensing flow by greater than 1 K.

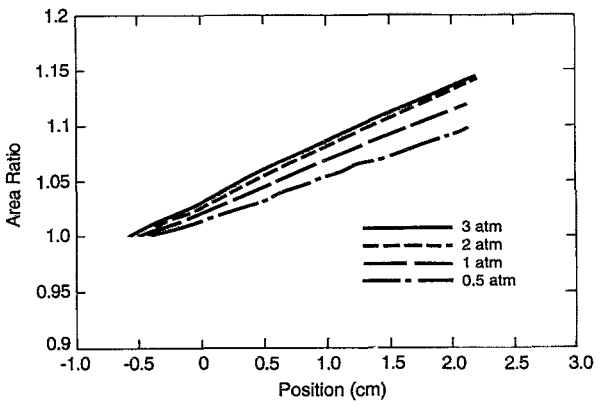

FIG. 6. Experimentally derived area ratios as a function of pressure.

TABLE I. Conditions at onset as a function of the stagnation pressure.

(a) Water, p_c=17.2 Torr, T_0=316 K

p_0 (atm)	T_{onset} (K)	$p_{c,onset}$ (Torr)
0.5	235	6.15
0.5	236	6.21
0.5	236	6.20
0.5	234.5	6.04
0.5	234	6.00
0.5	235	6.07
0.5	236	6.14
1.0	236	6.16
1.0	234	6.03
1.0	236	6.14
1.0	234	5.89
1.0	234	5.98
2.0	233.5	5.98
2.0	234	6.01
2.0	233.5	5.95
2.0	232.5	5.90
2.0	235	6.03
3.0	233.5	5.94
3.0	233.5	5.92
3.0	232.5	5.82

(b) Ethanol, p_c=12.8 Torr, T_0=316 K

p_0 (atm)	T_{onset}(K)	p_{onset} (Torr)
1.0	237.5	4.60
1.0	235	4.43
1.0	238	4.65
2.0	235.5	4.50
2.0	235	4.47
3.0	231	4.21
3.0	234	4.36
3.0	233.5	4.38

Table I summarizes the experimental conditions at onset. The value of $P_{c,onset}$ is taken from the integrated condensing flow pressure curve at the location corresponding to T_{onset}. Figures 7(a) and 7(b) show the onset temperatures versus total stagnation pressure for water and ethanol. At each pressure of interest we ran 3 to 8 experiments and determined the onset temperature to the closest 0.5 K. Different symbols distinguish experiments that have the same onset temperature. More experiments were completed at the lowest pressures to get better statistics. Each experiment consisted of one set of runs with N_2 to calibrate the nozzle followed by one set of runs with the desired level of condensible vapor. At a given total pressure, onset temperatures all lay within about 2 K of each other for water and within 3 K of each other for ethanol. Theoretical onset temperatures, calculated using the procedure outlined in Sec. IV, are also plotted.

Clearly the data and the theoretical trend are consistent with onset temperature increasing as the total pressure decreases. Although at the lowest pressures the fluctuating profiles make it harder to compare the isentropic regions of the

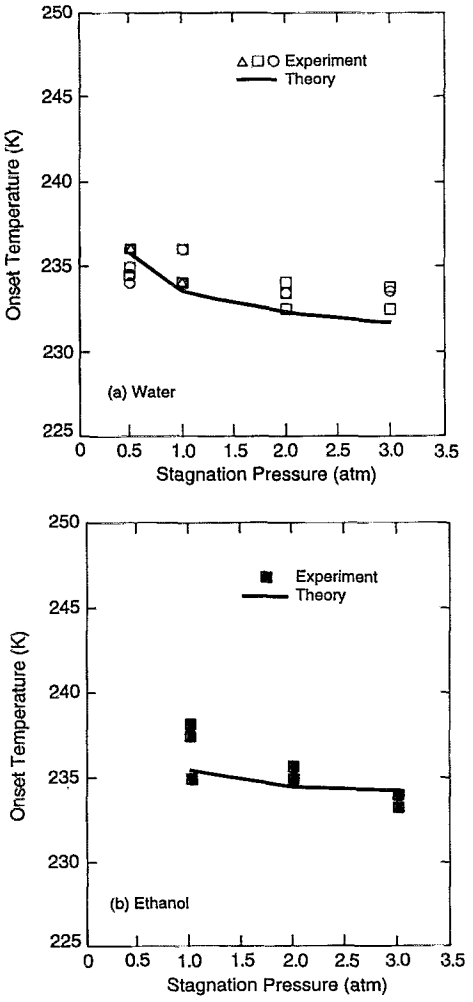

FIG. 7. Experimental and theoretical onset temperatures versus total stagnation pressure for $T_0=316$ K (a) water, $p_c=17.2$ Torr and (b) ethanol, $p_c=12.8$ Torr.

dry and condensing flows, the final sharp departure from the isentrope indicates that the upstream fluctuations are due to noisy interferograms. By choosing onset on the sharply departing curve we are finding the lowest possible onset temperature. These low values are still higher than or equal to the onset temperatures found at higher pressures, contrary to expectations based on limited energy transfer.

IV. CONDENSATION MODELING AND DISCUSSION

The theoretical calculations of condensation in the nozzle were performed using an integral steady state (ISS) model developed by Oswatitsch.[1] This model simulates the nucleation and growth of particles and includes the effects of heat addition to the flow through the diabatic gasdynamics equations.[2,3] The model is based on the classical kinetic model of cluster formation which considers cluster size to change only by monomer condensation and evaporation.[43] The steady state nucleation rate J is used to compute the number density ΔN of new particles formed at each point x in the expansion from the conservation law, $\Delta N=(J/u)\Delta x$; u is the local flow velocity. With an appropriate droplet growth law the condensate mass fraction can be calculated

TABLE II. Physical properties of water and ethanol (T is in K).

(a) Water	
$p_\infty(T)=610.483\left(\frac{273.2}{T}\right)^{5.1409}\exp\left(24.974\frac{(T-273.2)}{T}\right)$ (Pa)	Ref. 44
$\sigma(T)=118.44-0.155T$ (mN/m)	Ref. 45
$\Delta H_{vap}=2557$ (kJ/kg); $\rho_c=990$ (kg/m^3) at 250 K	Ref. 46
(b) Ethanol	
$\log_{10} p_\infty(T)=9.760-\frac{2372}{T}$ (Torr)	Ref. 4
$\sigma(T)=23.97-0.085T$ (mN/m)	Ref. 4
$\Delta H_{vap}=975$ (kJ/kg); $\rho_c=850$ (kg/m^3) at 223 K	Ref. 4

versus x, and from this the change in flow properties can be obtained by integrating the diabatic flow equations using the measured nozzle profile. This approach has been used extensively for simulating condensation in nozzles.[1–9] In our calculations, the classical isothermal steady state rate expression, J_{cl}, was used for J. Following conventional practice,[3–5] a multiplicative adjustment factor Γ was used to bring the calculated and measured values of the onset temperature into agreement. Thus J is expressed as $J=\Gamma J_{cl}$, where we use the following expression[3] for J_{cl}:

$$J_{cl}=\left(\frac{2\sigma\mu_v}{\pi N_A}\right)^{1/2}\left(\frac{p_v}{k_BT}\right)^2\frac{1}{\rho_c}\exp\left[-\frac{16\pi}{3}\left(\frac{\sigma}{k_BT}\right)^3\left(\frac{v_c}{\ln S}\right)^2\right]. \tag{12}$$

Here, σ, v_c, and ρ_c are the surface tension, molecular volume, and density of the condensate, respectively; p_v is the partial pressure of the condensible vapor; N_A is Avogadro's number, and k_B is the Boltzmann constant. In general, Γ varies with experimental conditions, but for a given expansion it is a temperature independent constant. An alternative method for achieving agreement between theory and experiment was introduced by Young[7] who used the classical nucleation expression in conjunction with a nonisothermal droplet growth law and adjustable condensation and evaporation coefficients. For the purposes of this work, the conventional approach should be adequate. We used the same droplet growth law as Wegener *et al.*[4] with the mass accommodation coefficient equal to one and the droplet temperature equal to the local gas temperature. The physical property data for water and ethanol used in the modeling are given in Table II. We also assumed that the mean axial velocity of the droplets equals the mean flow velocity of the expanding gas at each point in the nozzle. This assumption is justified by the large value of the slip number[47] (SLPN>300) for the largest particles (20 nm diameter) formed in our nozzle. The assumption is even better for the smaller particles.

In modeling the condensation of water we assumed that the subcooled particles were liquid droplets rather than ice. Because the surface tension of ice is so much larger than that of liquid water, nucleation rates for liquid drops always greatly exceed those of ice particles in accordance with Ostwald's law of stages. Recent analyses of moist air expansions in slender nozzles provide the best agreement with experiment when liquid droplets are assumed to form.[48,49] Older

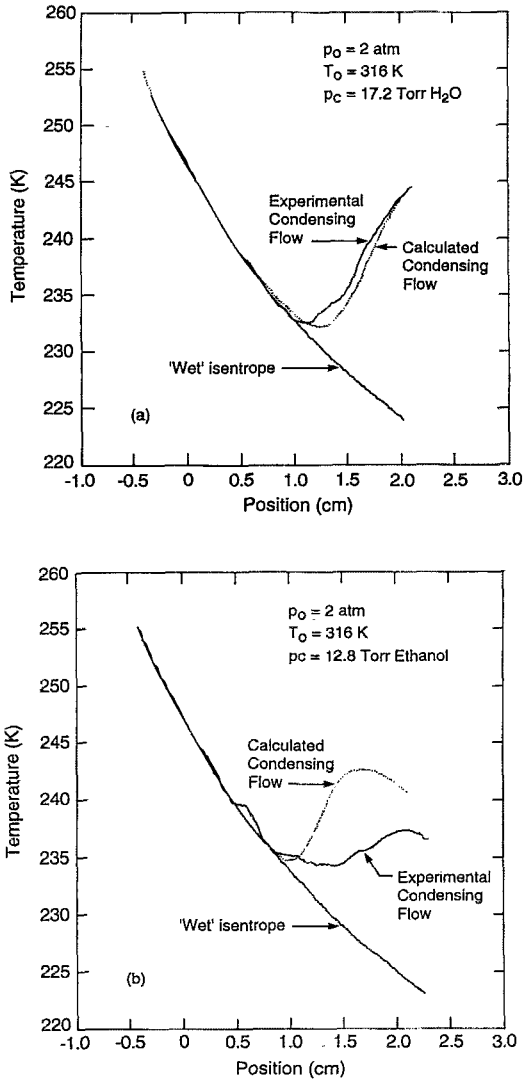

FIG. 8. Comparison of experimental temperature profiles with those predicted for condensation in the supersonic nozzle with $\Gamma=1$ for (a) water and (b) ethanol. The stagnation pressure p_0, temperature T_0, and condensible pressure p_c, for each experiment are listed in the figure.

expansion cloud chamber results of Anderson *et al.*[50] were consistent with homogeneous nucleation of liquid drops followed by freezing of the drops when the temperatures were low enough. Our own estimates of ice nucleation rates in a liquid drop show that drop freezing is entirely negligible during the 50 μs flow time from condensation onset to the nozzle exit.

Figures 8(a) and 8(b) illustrate that at 2 atm the isothermal model with $\Gamma=1$ adequately predicts onset for both water and ethanol experiments. The agreement with the water data is very good while for ethanol the rate of condensation downstream of onset is overpredicted. Since nucleation terminates rapidly after onset, this discrepancy can be attributed to our use of an isothermal growth law with perfect mass accommodation. The value of Γ was therefore fixed, and only the experimental area ratios were used to predict the expected behavior at each pressure. Changing the nucleation rate by a factor of 10 in the modeling results in a 3 K shift in the onset temperature. Thus large changes (>100×) in the experimental nucleation rate due to changes in carrier gas pressure should be readily observed. Furthermore, a decrease in the nucleation rate would lead to a decrease in the onset temperature as would a decrease in the droplet growth rate. This is opposite to what is observed experimentally and theoretically. The slight increase in onset temperature with decreasing pressure is consistent with the corresponding change in the heat capacity of the flowing gas. A given amount of heat addition *per mass of flow* produces the same deviation from the isentrope independent of pressure. The absolute mass of condensate needed to produce the required heat release is proportional to the total flow pressure for dilute mixtures. At low carrier gas pressures, less condensate is required, and this reduced amount can be formed by some combination of lower nucleation rate and less droplet growth. Thus condensation onset is observed at slightly lower supersaturations or, equivalently, at slightly higher temperatures. This argument is expected to break down eventually as carrier gas pressures approach those of the condensible vapor, and energy transfer effects begin to dominate.

We have made the most optimistic assumptions possible (unit mass accommodation and no energy transfer limitations on nucleation rate or droplet growth) to predict the variation of onset temperature with pressure. While the agreement with experiment is not perfect, a significant reduction in the nucleation rate due to energy transfer limitations at low pressure would result in poorer agreement. A large reduction in the mass accommodation coefficient would translate the predicted onset curve to lower temperatures. Based on the results of Figs. 6 and 7, we conclude that the small observed variation in onset temperature is readily explained by classical isothermal nucleation theory and droplet growth in conjunction with the pressure dependence of the gas stream's heat capacity and the fluid mechanics of the nozzle flow. This variation is also qualitatively consistent with the difference [cf. Fig. 4(a)] between our lowest ethanol onset temperature and the highest value of Wegener, Clumpner, and Wu[4] since their experiments were performed with a stagnation pressure of 0.8 atm whereas ours were at 3 atm.

V. CONCLUSION

We performed supersonic nozzle experiments with a fixed water or ethanol vapor pressure and varying amounts of carrier gas to test the hypothesis that a reduction in carrier gas pressure would delay the onset of condensation to a lower temperature. We actually observed a slight increase in the onset temperature as the stagnation pressure was reduced from 3 to 0.5 atm. We argued that this shift was consistent with the small changes in effective nozzle shape and the variation in heat capacity of the flowing gas that occurred with changing the total pressure. We found no need to invoke energy transfer limitations for the nucleation kinetics to explain the experimental results. We conclude that strong nonisothermal nucleation effects are not apparent in our results despite onset pressures that are generally subatmospheric (0.2 to 1 atm).

ACKNOWLEDGMENTS

We greatly appreciate the earlier contributions of S. Scherzer, R. Waterhouse, J. J. Helble, and V. Pierce in developing the nozzle apparatus. This work was supported by the U.S. Department of Energy, Division of Engineering and Geosciences, Office of Basic Energy Sciences, under Contract No. DE-AC02-84ER13154 and Grant No. DE-FG02-92ER14257.

APPENDIX: GASDYNAMICS EQUATIONS FOR DIABATIC FLOW

Diabatic flow is inviscid flow with heat addition. In the present case, heat addition is due to condensation. There are many presentations of the basic equations describing diabatic flow.[2,3,5–7] The development given here is designed to take advantage of the special characteristics of our experimental data. There are four equations to characterize the flow: continuity, momentum, energy, and the equation of state. The continuity and momentum equations are not formally affected by condensation; the energy equation and the equation of state are, and allowance must be made in them for the presence of condensate. The continuity equation is

$$\rho u A = \text{const}, \tag{A1}$$

where u is the local flow velocity, A is the local cross-sectional area of the nozzle, and ρ is the total density of the flowing gas including the condensate

$$\rho = \rho_i + \rho_v + \rho_c' . \tag{A2}$$

Here, the subscripts i, v, and c refer to the inert carrier gas, the condensible vapor, and the condensate particles, respectively. With regard to the latter, ρ_c' is defined using the same flow volume as for ρ_i and ρ_v; ρ_c' should not be confused with the density of the condensed phase ρ_c. The momentum equation is

$$\rho u\, du = -dp, \tag{A3}$$

where p is the gas pressure. The energy equation is

$$c_p\, dT + u\, du = L(T) dg, \tag{A4}$$

where $L(T)$ is the latent heat of condensation at temperature T, g is the condensate mass fraction defined as ρ_c'/ρ, and c_p is the specific heat of the flow

$$c_p = (m_i c_{pi} + m_v c_{pv} + m_c c_{pc})/m, \tag{A5}$$

$$m = m_i + m_v + m_c, \tag{A6}$$

and m denotes mass.

We designate the initial mass fraction of condensible vapor as ω_0, and use the following definitions, $1-\omega_0 = m_i/m$, $g = m_c/m$, $\omega_0 - g = m_v/m$ so that the specific heat can be rewritten as

$$c_p = (1-\omega_0) c_{pi} + (\omega_0 - g) c_{pv} + g c_{pc} . \tag{A7}$$

Finally, treating the gas mixture plus condensate particles as an ideal gas, the equation of state can be written as

$$p = (\rho_i/\mu_i + \rho_v/\mu_v + \rho_c'/\mu_c) RT, \tag{A8}$$

where R is the molar gas constant and μ_α denotes the molecular weight of species α. Because μ_c is so much larger than either μ_i or μ_v, Eq. (A8) can be simplified as

$$p = \rho(1-g)(R/\mu)T, \tag{A9}$$

where

$$\frac{1-g}{\mu} = \frac{1-\omega_0}{\mu_i} + \frac{\omega_0 - g}{\mu_v} . \tag{A10}$$

Two other relations, $\rho_i = (1-\omega_0)\rho$ and $\rho_v = (\omega_0 - g)\rho$, were also used in simplifying Eq. (A8). In differential form, Eq. (A9) becomes

$$\frac{dp}{p} = \frac{d\rho}{\rho} + \frac{dT}{T} - w(g) dg, \tag{A11}$$

where

$$w(g) = \frac{\mu}{\mu_v (1-g)} . \tag{A12}$$

These equations may be manipulated into the following four equations more suitable for numerical integration. The sonic flow speed at the nozzle throat, u^*, will be used to scale the flow velocity. We will assume that no condensate is present at the throat, so that $u^* = (\gamma R T^*/\mu)^{1/2}$ where γ is the ratio of specific heats for an ideal gas, $1/\gamma = 1 - R/(\mu c_p)$ and * denotes the value at the throat. The first two equations allow us to evaluate $M^* = u/u^*$ and p directly from the experimentally measured density and area ratio

$$d\ \ln(M^*) = -d\ \ln(\rho/\rho_0) - d\ \ln(A/A^*), \tag{A13}$$

$$d(p/p_0) = -\gamma^* M^{*2} (T^*/T_0)(\rho/\rho_0) d\ \ln(M^*), \tag{A14}$$

while g is obtained by integrating the equation

$$\gamma \left(\frac{L(T)}{c_p T} - w(g) \right) dg = [1 + g(\gamma - 1)] d\ \ln\left(\frac{p}{p_0}\right) - \gamma d\ \ln\left(\frac{\rho}{\rho_0}\right), \tag{A15}$$

where, subscript "0" indicates a value at stagnation conditions.

Finally, with dg and $d(p/p_0)$ available, $d(T/T_0)$ can easily be found after combining Eqs. (A3) and (A4) to yield

$$c_p T_0 d(T/T_0) = (p_0/\rho) d(p/p_0) + L(T) dg. \tag{A16}$$

The calculation proceeds step-by-step downstream in the nozzle from the first valid density data point.

[1] K. Oswatitsch, "Kondensationserscheinungen in Überschalldüsen," Z. Angew. Math. Mech. **22**, 1 (1942).
[2] P. G. Hill, "Condensation of water vapour during supersonic expansion in nozzles," J. Fluid Mech. **25**, 593 (1966).
[3] P. P. Wegener, "Gasdynamics of expansion flows with condensation, and homogeneous nucleation of water vapor," in *Nonequilibrium Flows*, Part I, Vol. 1 of *Gasdynamics*, edited by P. P. Wegener (Marcel Dekker, New York, 1969), Chap. 4, p. 163.
[4] P. P. Wegener, J. A. Clumpner, and B. J. C. Wu, "Homogeneous nucleation and growth of ethanol drops in supersonic flow," Phys. Fluids **15**, 1869 (1972).
[5] P. P. Wegener and B. J. C. Wu, "Gasdynamics and homogeneous nucleation," Adv. Colloid. Interface Sci. **7**, 325 (1977).
[6] S. Kotake and I. I. Glass, "Flows with nucleation and condensation," Prog. Aerospace Sci. **19**, 129 (1981).
[7] J. B. Young, "The spontaneous condensation of steam in supersonic nozzles," PhysicoChem. Hydrodynam. **3**, 57 (1982).

[8]L. S. Bartell, "Supplementary analyses in diffraction studies of clusters. Computer modeling of nucleation and growth," J. Phys. Chem. **94**, 5102 (1990).
[9]P. P. Wegener and A. A. Pouring, "Experiments on condensation of water vapor by homogeneous nucleation in nozzles," Phys. Fluids **7**, 352 (1964).
[10]D. Barschdorff, "Carrier gas effects on homogeneous nucleation of water vapor in a shock tube," Phys. Fluids **18**, 529 (1975).
[11]B. J. C. Wu, P. P. Wegener, and G. D. Stein, "Condensation of sulfur hexafluoride in steady supersonic nozzle flow," J. Chem. Phys. **69**, 1776 (1978).
[12]M. W. Matthew and J. Steinwandel, "An experimental study of argon condensation in cryogenic shock tubes," J. Aerosol Sci. **14**, 755 (1983).
[13]J. Steinwandel and T. Buchholz, "Homogeneous condensation of argon: An experimental study using the nozzle flow of a cryogenic Ludwieg tube," Aerosol Sci. Tech. **3**, 71 (1984).
[14]J. Steinwandel, "Homogeneous condensation of nitrogen in the expansion wave of a cryogenic shock tube," Ber. Bunsenges. Phys. Chem. **89**, 481 (1985).
[15]A. Kantrowitz, "Nucleation in very rapid vapor expansions," J. Chem. Phys. **19**, 1097 (1951).
[16]J. Feder, K. C. Russell, J. Lothe, and G. M. Pound, "Homogeneous nucleation and growth of droplets in vapor," Adv. Phys. **73**, 1584 (1966).
[17]E. E. Salpeter, "Heat transfer in nucleation theory," J. Chem. Phys. **58**, 4331 (1973).
[18]J. M. Soler and N. Garcia, "Nonequilibrium internal and translational temperature of clusters in homogeneous nucleation," Phys. Rev. A **27**, 3300 (1983).
[19]I. J. Ford and C. F. Clement, "The effects of temperature fluctuations in homogeneous nucleation theory," J. Phys. A **22**, 4007 (1989).
[20]C. F. Clement, "Growth processes and homogeneous nucleation in vapor–gas mixtures," in *Atmospheric Aerosols and Nucleation*, Lecture Notes in Physics, edited by P. E. Wagner and G. Vali (Springer-Verlag, Berlin, 1988), Vol. 309, pp. 364–366.
[21]J. C. Barrett, C. F. Clement, and I. J. Ford, "Energy fluctuations in homogeneous nucleation theory for aerosols," J. Phys. A **26**, 529 (1993).
[22]B. E. Wyslouzil and J. H. Seinfeld, "Nonisothermal homogeneous nucleation," J. Chem. Phys. **97**, 2661 (1992).
[23]J. L. Katz, C.-H. Hung, and M. Krasnopoler, "The homogeneous nucleation of nonane," in *Atmospheric Aerosols and Nucleation*, Lecture Notes in Physics, edited by P. E. Wagner and G. Vali (Springer-Verlag, Berlin 1988), Vol. 309, pp. 356–359; J. L. Katz, J. A. Fisk, and V. Chakarov, "The accuracy of nucleation theory," in *Nucleation and Atmospheric Aerosols*, edited by N. Fukuta and P. E. Wagner (Deepak, Hampton, VA, 1992), pp. 11–18.
[24]M. P. Anisimov and S. N. Vershinin, "Dibutylphtalate nucleation rate at carbon-dioxide different pressures," J. Aerosol. Sci. **21**, S11 (1990); "Dibutylphtalate vapor heteromolecular nucleation in helium atmosphere," *ibid.* **21**, S15 (1990).
[25]P. E. Wagner, R. Strey, and Y. Viisanen, "The effect of carrier gas pressure on homogeneous nucleation rates in supersaturated vapors," in *Nucleation and Atmospheric Aerosols*, edited by N. Fukuta and P. E. Wagner (Deepak, Hampton, VA, 1992), pp. 27–29.
[26]G. Wilemski, B. E. Wyslouzil, M. Gauthier, and M. B. Frish, "Effect of carrier gas pressure on water condensation in a supersonic nozzle," in *Nucleation and Atmospheric Aerosols*, edited by N. Fukuta and P. E. Wagner (Deepak, Hampton, VA, 1992), pp. 23–26.
[27]H. W. Leipman and A. Roshko, *Elements of Gasdynamics* (Wiley, New York, 1957).
[28]R. Ladenburg and D. Bershader, "Interferometry," in *Physical Measurements in Gasdynamics and Combustion*, edited by R. Ladenburg (Princeton University Press, Princeton, NJ, 1954), Part 1.
[29]E. Hecht and A. Zajac, *Optics* (Addison–Wesley, Reading, MA, 1975).
[30]R. C. Reid, J. M. Prausnitz, and B. E. Poling, *The Properties of Gas and Liquids*, 4th ed. (McGraw-Hill, New York, 1987), pp. 407–410.
[31]J. R. Welty, C. E. Wicks, and R. E. Wilson, *Fundamentals of Momentum, Heat, and Mass Transfer*, 2nd ed. (Wiley, New York, 1976), p. 738.
[32]R. H. Perry and C. H. Chilton, *Chemical Engineer's Handbook*, 5th ed. (McGraw-Hill, New York, 1973), pp. 210–211.
[33]D. B. Dawson, E. J. Willson, P. G. Hill, and K. C. Russell, "Nucleation of supersaturated vapors in nozzles, II. C_6H_6, $CHCl_3$, CCl_3F, and C_2H_5OH," J. Chem. Phys. **51**, 5389 (1969).
[34]F. Peters, "Homogeneous nucleation of ethanol and *n*-propanol in a shock tube," J. Chem. Phys. **77**, 4788 (1982).
[35]J. P. Franck and H. G. Hertz, "Messung der kritischen Übersättigung von Dämpfen mit der Diffusionsnebelkammer," Z. Phys. **143**, 559 (1956).
[36]J. L. Katz and B. J. Ostermeier, "Diffusion cloud-chamber investigation of homogeneous nucleation," J. Chem. Phys. **47**, 478 (1967).
[37]A. A. Pouring, "An experimental and analytical investigation of homogeneous condensation of water vapor in air during rapid expansion," Ph.D. thesis, Yale University, New Haven, CT, 1963.
[38]R. Roberts, "A light scattering investigation of droplet growth in nozzle condensation," Report No. 97, MIT, Gas Turbine Lab, Cambridge MA, 1969.
[39]G. D. Stein and C. A. Moses, "Rayleigh scattering experiments on the formation and growth of water clusters nucleated from vapor phase," J. Colloid Interface Sci. **39**, 504 (1972).
[40]G. D. Stein, "Condensation of ice clusters by homogeneous nucleation from the vapor phase," Ph.D. thesis, Yale University, New Haven, CT, 1967.
[41]G. Wilemski, B. E. Wyslouzil, M. G. Beals, and M. B. Frish (in preparation); a preliminary discussion is available in G. Wilemski, B. E. Wyslouzil, M. Gauthier, and M. B. Frisch, "Effect of carrier gas pressure on condensation in a supersonic nozzle," in *Proceedings of the Eleventh Symposium on Energy Engineering Sciences*, Argonne, Illinois, May 1993 (NTIS CONF-9305134) (1993), pp. 56–62.
[42]H. S. Stever, "Condensation in high speed flows," in *Fundamentals of Gasdynamics*, edited by H. W. Emmons (Princeton University Press, Princeton, NJ, 1958), pp. 526–573.
[43]F. F. Abraham, *Homogeneous Nucleation Theory* (Academic, New York, 1974).
[44]H. L. Jaeger, E. J. Willson, P. G. Hill, and K. C. Russell, "Nucleation of supersaturated vapors in nozzles, I. H_2O and NH_3," J. Chem. Phys. **51**, 5380 (1960).
[45]D. E. Hagen and J. L. Kassner, Jr., "Homogeneous nucleation rate for water," J. Chem. Phys. **81**, 1916 (1984).
[46]H. R. Pruppacher and J. D. Klett, *Microphysics of Clouds and Precipitation* (Reidel, Dordrecht, 1980), p. 89.
[47]M. H. Schwartz and R. P. Andres, "Theoretical basis of the time-of-flight aerosol spectrometer: A method for monitoring the size distribution of submicron aerosol particles," J. Aerosol Sci. **7**, 281 (1976).
[48]C. F. Delale, G. H. Schneer, and J. Zierep, "Asymptotic solution of transonic nozzle flows with homogeneous condensation. I. Subcritical flows," Phys. Fluids A **5**, 2969 (1993).
[49]C. F. Delale, G. H. Schneer, and J. Zierep, "Asymptotic solution of transonic nozzle flows with homogeneous condensation. II. Supercritical flows," Phys. Fluids A **5**, 2982 (1993).
[50]R. J. Anderson, R. C. Miller, J. L. Kassner, Jr., and D. E. Hagen, "A study of homogeneous condensation-freezing nucleation of small water droplets in an expansion cloud chamber," J. Atmos. Sci. **37**, 2508 (1980).